MOTION ANALYSIS OF A LINEAR VIBRATORY FEEDER: DYNAMIC MODELING AND EXPERIMENTAL VERIFICATION

Marco Buzzoni[a,b], Mattia Battarra[a,c,*], Emiliano Mucchi[a,d], Giorgio Dalpiaz[a,e]

[a]*Engineering Department, University of Ferrara, Via Saragat, 1 I-44122 Ferrara, Italy*
[b]*marco.buzzoni1@unife.it*
[c]*mattia.battarra@unife.it*
[d]*emiliano.mucchi@unife.it*
[e]*giorgio.dalpiaz@unife.it*

Abstract

The mathematical model for evaluating the dynamic behavior of linear vibratory feeders is presented and discussed. The model is based on the Eksergian's equation of motion, with the aim at taking into account the effects of the main design parameters without unnecessarily increasing the complexity of the model. Deep emphasis is given to the procedure for the estimation of the external excitations applied to the driveline by proposing two procedures. The first one gives birth to a transcendent equation system, while the second procedure, based on more restrictive hypotheses regarding the geometry of the feeder, leads to a linear system. A dedicated experimental campaign for characterizing the dynamic behavior of a real machine is conducted under different operational conditions. Measured data are compared with simulated results obtained by applying both models; the experimental validation highlights the satisfactory quality of the model estimation, both in terms of torsional oscillations of the driveline and frame vibrations.

Keywords: linear feeder, dynamic model, torsional vibrations, experimental validation

1 Introduction

The vibratory feeders exploit the shaking motion in order to guarantee the proper carriage of the small parts during the industrial process. These machines can be classified into three main categories [1], depending on the excitation nature: electromechanical, electromagnetic and purely mechanical. They are broadly used in a wide range of industrial applications, as the automated assembly or the food processing, and therefore they are generally conceived considering specific requirements depending on the applications. For this reason, the project of the vibratory feeders is particularly challenging since the identification of the significant design parameters can be carried out only with a priori estimation of their dynamic behavior.

A number of works present in the specialized literature acknowledges the significant interest of the investigations on the vibratory feeders, mainly involving topics as the dynamic modeling and the motion control. Regarding the dynamic modeling, Mucchi et al. [2], Ding and Dai [3] and Despotovic et al. [4] developed a dynamic model of a vibratory feeder for the estimation of the natural frequencies in order to provide the framework for design guidelines. Moreover, Silversides et al. [5] focused on the theoretical estimation of the forces involved in the operational conditions. Other works address the study of the

*Corresponding author

interactions between the carried parts and the feeder by analytical approaches [6–11] and numerical ones [12], with the main purpose of estimating the mean conveying velocity. The control of the feeders actuators [13–15] is another prominent aspect due to its active influence on the overall performance of these machines.

In the presented work, a mechanical linear feeder with three horizontal parallel frames has been investigated in terms of its dynamic behavior during operational conditions departing from a previous preliminary model previously presented in [16]. In particular, the proposed approach focuses on the development of a torsional dynamic model that allows for the prediction of the speed and acceleration fluctuations of the feeder's driveline. Although the apparent simplicity of the mechanism, this machine intrinsically own a complexity since the actuator, i.e. an asynchronous motor, does not have an active torque control system. These characteristics cause the external torques involved in the operational conditions to change continuously, according to the dynamic behavior of the driveline and several design parameters. In order to demonstrate the quality of the estimation, results provided by the model have been compared with measured data obtained from a dedicated experimental campaign, both in terms of torsional oscillations of the driveline and global vibration of each frame.

Most previous studies regard the development of dynamics model focusing on the estimation of the natural frequencies or the motion of the carried parts. The originality of the proposed approach mainly resides in the dynamic modeling of the feeder driveline that acts a crucial role on the overall performance of this particular kind of vibratory feeder. Moreover, as far as the authors are aware, no dynamic models of this type of linear vibratory feeders have been already introduced in the literature. Therefore, the presented work deals with a torsional dynamic modeling of a linear vibratory feeder driven by an asynchronous motor, having a generic mathematical formulation in order to taking into account arbitrary design and geometrical data.

The paper is organized as follows: Section 2 presents the dynamic model, Section 3 describes the experimental setup, Section 4 regards the model assessment by means of experimental measurements and Section 5 draws the final remarks.

2 Dynamic model

The present section is focused on the description of the main components that constitute the mechanical system and the mathematical model adopted to evaluate its dynamic behavior. Subsection 2.1 is then centered on describing the procedure for evaluating the opposing torque due to the presence of leaf springs.

Figure 1 shows the main components being part of the mechanism of a linear feeder. Two parallel frames, which are used to move the pieces of pasta along the production line, are connected to the machine body by means of 24 leaf springs bolted on them, 12 for each frame. Concurrently, each frame is moved by a couple of parallel rods, which link the respective frame to an eccentric elements directly shaped on the common shaft; the four eccentric elements are designed so that the two frames move in counter phase with respect to each other. It is therefore clear that the shaft, together with the two eccentric elements, can be considered as the crankshaft of the mechanism. Finally, an electric motor (asynchronous motor) drives the whole system through a trapezoidal belt transmission.

The described mechanism has been divided in two subsystems, each one analyzed with a purely torsional approach: subsystem #1 referring to the engine shaft and subsystem #2 referring to the crankshaft. Therefore, by following the scheme shown in Figure 2, the Eksergian's equation of motion [17,18] can be applied to each subsystem:

$$J_1\ddot{\theta}_1 + \tfrac{1}{2} J_1'\dot{\theta}_1^2 = M_m + \left(T_f - T_b\right)R_1 \tag{1}$$

$$J_2\ddot{\theta}_2 + \tfrac{1}{2} J_2'\dot{\theta}_2^{\,2} = M^* + \left(T_b - T_f\right)R_2 \tag{2}$$

where θ_1 and θ_2 define the instantaneous angular position of the driving shaft and the crankshaft, respectively; R_1 and R_2 are the radius of the pulleys on the motor side and the crankshaft side, respectively; while T_f and T_b represent the belt tension on the two sides of each pulley. Regarding the inertia terms, J_1 is the global polar mass moment of inertia on the motor side, given by the sum of the inertia of the electric motor $J_{1,m}$ and the inertia of the pulley $J_{1,p}$, while J_2 accounts for all the contributions related to the crankshaft side. In particular, J_2 can be expressed as follows:

$$J_2 = J_2^I\left(\theta_2\right) + J_2^{II}\left(\theta_2\right) + J_{2,s} + J_{2,p} + J_0 + m_r e^2 \tag{3}$$

where $J_{2,s}$ is the polar mass moment of inertia of the crankshaft, $J_{2,p}$ is the polar mass moment of inertia related to the pulley, J_0 and $m_r e^2$ are the inertia terms related to the connecting rods, while J_2^I and J_2^{II} represent the polar mass moment of inertia related to the two parallel moving frames respectively. It is fundamental to be noted that the alternative motion of the two frames makes terms J_2^I and J_2^{II}, and therefore the global term J_2, being dependent on crankshaft angular position θ_2; the determination of the kinematic law linking J_2^I and J_2^{II} to θ_2 will be analyzed in subsection 2.1. On the contrary, polar mass moment J_1 does not depend on the driving shaft angular position θ_1. Finally, terms M_m and M^* represent the generalized torques applied to the system. In particular, M_m is the driving torque, which is typically provided by a three-phase asynchronous motor. Hence, taking advantage of the common assumption that, within the designed working condition range, a linear relationship between torque and speed exists, M_m can be expressed as:

$$M_m = k_m\left(\Omega_s - \dot{\theta}_1\right) \tag{4}$$

where Ω_s is the stator electrical speed and k_m is the angular coefficient related to the mechanical characteristics of the adopted motor. The last term to be considered is torque M^*, which is defined as a generalized torque acting on the crankshaft; torque M^* takes into account the elastic reaction of the leaf springs M_e and the weight of the moving frames M_w:

$$M^* = M_e + M_w \tag{5}$$

As observed about terms J_2^I and J_2^{II} in Eqn.(3), both torque contributions M_e and M_w depend on the crankshaft angular position θ_2, therefore the procedure for their estimation will be given in subsection 2.1.

The terms representing the belt tension can be now expressed with respect to their dependence on the instantaneous position of the two shafts:

$$R_1\left(T_f - T_b\right) = 2cR_1(\dot{\theta}_1 R_1 - \dot{\theta}_2 R_2) + 2kR_1(\theta_1 R_1 - \theta_2 R_2) \tag{6}$$

where $\theta_1 R_1 - \theta_2 R_2$ represents the instantaneous transmission error between the two pulleys that constitute the belt transmission, k and c are the stiffness and damping coefficient of the trapezoidal belt. Therefore, Eqns. (1) and (2) can be rewritten and joined in the following equation system:

$$\begin{cases} J_1\ddot{\theta}_1 + 2cR_1(\dot{\theta}_1R_1 - \dot{\theta}_2R_2) + 2kR_1(\theta_1R_1 - \theta_2R_2) = k_m\left(\Omega_s - \dot{\theta}_1\right) \\ J_2\ddot{\theta}_2 + \frac{1}{2}J_2'\dot{\theta}_2^2 - 2cR_2(\dot{\theta}_1R_1 - \dot{\theta}_2R_2) - 2kR_2(\theta_1R_1 - \theta_2R_2) = M_e + M_w \end{cases} \quad (7)$$

It is worth underlining that Eqn. (7) represents a semi-definite system that could be reduced to a single degree of freedom equation with a different definition of the unknowns; therefore, the hypotheses allowing for the application of the Eksergian's equation are fully satisfied.

2.1 Evaluation of the generalized torques

In the present subsection, attention is focused on determining the torque components (see Eqn.(5)) and the polar mass moment of inertia components (see Eqn. (3)) that depend on crankshaft angular position θ_2; the procedure will be based on the calculation of the VCs [18] (velocity coefficients) S_x and S_y that characterize the mechanism used to drive the two parallel moving frames.

With respect to the global reference system defined in Figure 3, Eqn.(3) may be rearranged in order to explicit the inertia components J_2^I and J_2^{II} in terms of their dependence on S_x and S_y:

$$J_2 = m^I\left[\left(S^I{}_x\right)^2 + \left(S^I{}_y\right)^2\right] + m^{II}\left[\left(S^{II}{}_x\right)^2 + \left(S^{II}{}_y\right)^2\right] + J_{2,s} + J_{2,p} + J_0 + m_r e^2 \quad (8)$$

where m^I and m^{II} represent the mass of the two moving frames. The same approach can be applied to torque components M_e and M_w leading to Eqns. (9)-(10):

$$M_w = m^I g S_y{}^I + m^{II} g S_y{}^{II} \quad (9)$$

$$M_e = F_x{}^I S_x{}^I + F_y{}^I S_y{}^I + F_x{}^{II} S_x{}^{II} + F_y{}^{II} S_y{}^{II} \quad (10)$$

where F_x and F_y represent the leaf spring elastic reactions in the global reference system, namely xy, whereas g is the acceleration of gravity. Such reactions can be expressed also in terms of the leaf springs equivalent stiffness:

$$M_e = (k_{xx}x_{P^I} + k_{xy}y_{P^I})S^I{}_x + (k_{xy}x_{P^I} + k_{yy}y_{P^I})S^I{}_y + (k_{xx}x_{P^{II}} + k_{xy}y_{P^{II}})S^{II}{}_x + (k_{xy}x_{P^{II}} + k_{yy}y_{P^{II}})S^{II}{}_y \quad (11)$$

where stiffness terms k_{xx}, k_{xy} and k_{yy} are explained in detail in Eqn. (18).

Therefore, in order to estimate the VCs and the leaf spring reaction, it is first necessary to determine the law linking the displacement of the frames, namely x_P and y_P, and the angular position of the crankshaft θ_2. The procedure has been obtained according to the scheme shown in Figure 3, representing the feeder at the time instant where the leaf springs are not deformed. The proposed methodology is based on the following hypotheses:

- frame I and frame II have been considered as points with mass P^I and P^{II}, respectively. The green and blue planes in Figure 3 represent the planes where P^I and P^{II} can move;
- since in the real system each frame is connected to the structural base by 12 leaf springs, the proposed model considers a single leaf spring with an equivalent stiffness for each frame;
- the other mechanical components, i.e. the rods and eccentrics, are perfectly rigid.

For each frame i, the first step is to estimate its displacement in the xy plane. Departing from the present vector identity:

$$\mathbf{P}^i + \left(\mathbf{Q}^i - \mathbf{P}^i\right) = \mathbf{C}^i + \left(\mathbf{Q}^i - \mathbf{C}^i\right) \tag{12}$$

Thus, the coordinates of P^i in the xy plane, namely x_{P^i} and y_{P^i} can be obtained:

$$\begin{cases} x_{P^i} = x_{Q^i} - b\cos\alpha^i \\ y_{P^i} = y_{Q^i} - b\sin\alpha^i \end{cases} \tag{13}$$

where x_{Q^i} and y_{Q^i} are defined as

$$\begin{aligned} x_{Q^i} &= \sqrt{b^2 - e^2} + c\cos\theta_2 \\ y_{Q^i} &= e\sin\theta_2 \end{aligned} \tag{14}$$

Equation (13) represents an undetermined problem, being constituted by two equations and three unknowns (x_{P^i}, y_{P^i} and α^i), therefore a third equation, i.e. the equilibrium of moments, needs to be introduced. The torques due to the elastic actions in point P with respect to point Q can be defined as:

$$(\mathbf{P}^i - \mathbf{Q}^i) \times \mathbf{F}^i = \begin{vmatrix} u & v & w \\ x_{P^i} - x_{Q^i} & y_{P^i} - y_{Q^i} & 0 \\ F_x{}^i & F_y{}^i & 0 \end{vmatrix} \tag{15}$$

where u, v, and w are the standard basis related to directions x, y and z, respectively. Hence, the equilibrium of moments can be written as:

$$F_y{}^i (x_{P^i} - x_{Q^i}) - F_x{}^i (y_{P^i} - y_{Q^i}) = 0 \tag{16}$$

The elastic actions, namely $F^i{}_x$ and $F^i{}_y$, are evaluated with the following equation:

$$\mathbf{F}^i = \mathbf{R}\mathbf{K}^i\mathbf{R}^{-1}\mathbf{s}^i \tag{17}$$

where $\mathbf{F}^i$ is the elastic action vector in global reference system xy, $\mathbf{K}^i$ is the stiffness matrix in the local reference system, $\mathbf{s}^i$ is the displacement vector in the global reference system and $\mathbf{R}$ is the rotation matrix. For the sake of completeness, $\mathbf{F}^i$, $\mathbf{K}^i$, $\mathbf{s}^i$ and $\mathbf{R}$ are reported hereafter:

$$
\begin{aligned}
&\mathbf{F}^i = \begin{Bmatrix} F_x{}^i \\ F_y{}^i \end{Bmatrix} \\
&\mathbf{K}^i = 12\begin{bmatrix} k_{xx} & k_{xy} \\ k_{xy} & k_{yy} \end{bmatrix} = 12\begin{bmatrix} EA/a & 0 \\ 0 & 12EJ/a^3 \end{bmatrix} \\
&\mathbf{s}^i = \begin{Bmatrix} x_{P^i} \\ y_{P^i} \end{Bmatrix} \\
&\mathbf{R} = \begin{bmatrix} \cos(\gamma^i - \pi/2) & \sin(\gamma^i - \pi/2) \\ -\sin(\gamma^i - \pi/2) & \cos(\gamma^i - \pi/2) \end{bmatrix}
\end{aligned}
\tag{18}
$$

Finally, Equation (16) can be added to equation system (13), obtaining

$$
\begin{cases}
x_{P^i} = x_{Q^i} - b\cos\alpha^i \\
y_{P^i} = y_{Q^i} - b\sin\alpha^i \\
F_y{}^i(x_{P^i} - x_{Q^i}) - F_x{}^i(y_{P^i} - y_{Q^i}) = 0
\end{cases}
\tag{19}
$$

which is now a determined system giving the position of frame i as a function of θ_2. It has to be noted that the third equation in Eqn. (19) is transcendent, therefore Eqn. (19) must be solved numerically. The procedure can be equally applied to frame I and II; moreover, it would be still valid for linear feeders with a single frame mechanism or more than two.

The procedure from Eqn. (12) to (19) can be further simplified if the geometry of the linear feeder under study allows for the application of two more hypotheses. In particular, by assuming:

- α sufficiently close to zero, i.e. the e/b ratio is small;
- stiffness component k_{xx} in the local reference system of some orders of magnitude higher than stiffness component k_{yy};

then the trajectory followed by P^i tends to collapse into a straight line and:

$$
\begin{aligned}
&\sin\alpha \simeq \alpha \\
&\cos\alpha \simeq 1
\end{aligned}
\tag{20}
$$

which allows for the linearization of Equation (19). Indeed, the latter consideration about the stiffness values, de facto, transforms the kinematic constrain represented by the leaf spring into a prismatic joint moving along the orthogonal direction with respect to the leaf spring axis, i.e. y^I and y^{II} referring to Figure 3. Since the displacement of frame i, namely P^i, is allowed only along the y^i direction, the following relationship between the local reference system and the global one can be drawn as:

$$
\begin{cases}
x_{P^i} = y^i{}_{P^i}\cos\left(\gamma_A - \dfrac{\pi}{2}\right) \\
y_{P^i} = y^i{}_{P^i}\sin\left(\gamma_A - \dfrac{\pi}{2}\right)
\end{cases}
\tag{21}
$$

where $y_{P^i}^i$ is the displacement of frame i in the local reference system. Eventually, after a simple manipulation of Eqn. (21), the following relationship is obtained:

$$\frac{x_{P^i}}{y_{P^i}} = \frac{\cos\left(\gamma^i - \frac{\pi}{2}\right)}{\sin\left(\gamma^i - \frac{\pi}{2}\right)} \tag{22}$$

Equation (22) means that x_{P^i} and y_{P^i} are linked each other by a constant term. Hence, in agreement with the previous assumptions, Equation (19) can be simplified as a system of linear equations:

$$\begin{cases} x_{P^i} = x_{Q^i} - b \\ y_{P^i} = y_{Q^i} - b\alpha^i \\ \dfrac{x_{P^i}}{y_{P^i}} = \dfrac{\cos\left(\gamma^i - \frac{\pi}{2}\right)}{\sin\left(\gamma^i - \frac{\pi}{2}\right)} \end{cases} \tag{23}$$

where α^i, x_{P^i} and y_{P^i} are analytically expressed as a function of θ_2:

$$\alpha^i = \frac{e\sin\theta_2 - \dfrac{\left(\sin(\gamma^i - \pi/2)\right)\left(c\cos\theta_2 - b + \sqrt{b^2 - e^2}\right)}{\gamma^i - \pi/2}}{b} \tag{24}$$

$$x_{P^i} = e\cos\theta_2 - b + \sqrt{b^2 - e^2} \tag{25}$$

$$y_{P^i} = \frac{\sin(\gamma^i - \pi/2)\left(e\cos\theta_2 - b + \sqrt{b^2 - e^2}\right)}{\cos(\gamma^i - \pi/2)} \tag{26}$$

Unlike Eqn. (19), where x_{P^i} and y_{P^i} must be estimated numerically, the displacement of frame i can be exactly evaluated by Eqns. (25) and (26). Eventually, also the velocity and the acceleration can be analytically calculated as well as the VCs, making both the numerical implementation of the model and the post-processing of the results easier. Moreover, it has to be remembered that the estimation of the elastic torque M_e due to the leaf springs deformation may vary depending on the use of Eqn. (19) or Eqn. (23). By using Eqn. (19), the considered stiffness matrix will be the same as Eqn. (18) whereas using Eqn. (23), $\mathbf{K}^i$ will be:

$$\mathbf{K}^i = 12\begin{bmatrix} 0 & 0 \\ 0 & 12EJ/a^3 \end{bmatrix} \tag{27}$$

since, in this simplified subcase, the axial deformation of the leaf springs is neglected.

In conclusion, two formulations have been proposed by using different sets of assumptions. Both mathematical formulations have been implemented into the dynamic model and validated by experimental measurements.

3 Experimental analysis

The operational measurements are a pivotal step to experimentally characterize the mechanical system for a further model validation. The measure of the torsional vibration of the eccentric shaft, i.e. the instantaneous angular speed of the shaft, can be performed installing zebra tape on the shaft of interest coupled with an accurate tachometer. In this study, the test has been performed by means of an optical sensor type Optel Thevon 152 G7 GP RV4 equipped with probe Optel Thevon Multi Slit YO 6M HM6X80 SURG. The setup is depicted in Figure 4, where the sensor has been fixed to the structural base by a magnetic base while the zebra tape has been glued on the shaft. The zebra tape has line width of 2 mm and accounts a high number of lines in order to avoid aliasing effects and obtaining also a proper resolution for the torsional measurement. The torsional data has been acquired with a counting rate of 800 MHz by means of the acquisition system LMS SCADAS 305.

These experimental measurements have been carried out at different speeds in order to provide a robust and reliable model validation. Specifically, referring to the power line frequency, the tests has been performed at 35 Hz, 40 Hz, 45 Hz, 50 Hz (design working condition) and 55 Hz. The tested power line frequencies are referred to the following nominal speeds of the crankshaft: 252 rpm, 288 rpm, 324 rpm, 360 rpm and 369 rpm. It has to be underlined that the proposed model does not takes into account the effect of the carried product, therefore also the experimental tests have been performed without it. As an example of the experimental results, Figure 5 depicts measured instantaneous speed (on the left side) and the vibration signal of the frame I (on the right side) acquired at the working speed (360 rpm). It has to be noted that the torsional oscillation of the feeder has large fluctuations due to the high variability of the load combined to the mediocre torque control of the asynchronous motor.

Additionally, the vibration signatures of the feeder have been acquired with a sampling frequency of 1024 Hz by three triaxial piezoelectric accelerometers (PCB model 356B21) organized as shown in Figure 6. Accelerometers 1 and 2 have been glued on the frame I and II, respectively, whereas accelerometer 3 has been placed on the structural base.

4 Model validation and results

In the present section, results coming from the model introduced in section 2 are shown and discussed; in particular, priority will be given on the comparison with experimental results in order to demonstrate the quality of the estimation in terms of:

- comparison between waveforms in time domain;
- root mean square (RMS) of the first four harmonics;

Table 1 reports the main parameters referring to the linear feeder used for model validation and therefore adopted for running the simulations. Damping coefficient c has been chosen by setting the modal damping ζ equals to 1%; as observed in [2] by means of an extended experimental analysis, this is a reasonable reference value for this type of machine. Figure 7a shows the trajectory followed by points P^I and P^{II} in the global reference system, calculated by following the procedure from Eqn. (12) to (19), namely Original model, with the parameters defined in Table 1. As it can be observed, since the ratio e/b is particularly small (about 0.5%), the trajectory tends to collapse on a straight line. In fact, Figure 7b and Figure 7c, representing the trajectory of points P^I and P^{II} in their respective local reference system, highlight that the displacements substantially occur in the orthogonal axis of the leaf spring, namely y^I and y^{II}, being of three orders of magnitude higher than the displacements along the longitudinal axis, namely x^I and x^{II}.

Moreover, Figure 8 shows the variation of α along a complete revolution of the crankshaft for both frame I and II calculated by applying the Original model. It can be noted that the variation of α is significantly small. In light of what has been shown up to this point, the procedure from Eqn. (21) to (27), namely Simplified model, is suitable to be applied. As a further proof of the reasonability of the assumptions of the Simplified model, Figure 9 highlights the overlapping of the displacement values estimated by the two proposed approaches.

The presented data have been used to simulate five different working conditions, in order to replicate the experimental campaign described in Section 3. Figure 10 shows the comparison of the time domain waveforms between the measured instantaneous speed and the simulated one. In this comparison, the model results appear to be superposed to the experimental results in all the tested conditions. It has to be noted that the results of the Simplified model are satisfying as well as the Original model. This first approach allows for the overall validation of the phases and amplitudes of the obtained results, but a more precise comparison is needed for the proper assessment of the proposed model. With this purpose, the RMS value of the first four harmonics of the crankshaft angular speed has been calculated for both the experimental data and the simulated ones. Results are shown in Figure 11, where the top chart (Figure 11a) is used to evaluate the results obtained with the Original model, while the bottom chart (Figure 11b) depicts the results obtained with the Simplified model. As it can be observed, both the approaches guarantee a good level of accuracy; in particular, even if the Original model appears to give a whole better estimation, differences between the results of the two approaches are not so relevant.

Results provided by the model can also be used to evaluate the acceleration related to points P^I and P^{II}. Figure 12 shows the comparison between the model results and experimental one with regard to the RMS values of the frames accelerations. It can be observed that the results provided by the Original model are analogous with respect to the Simplified model ones; both of them show a general agreement with the measured data. Moreover, in this comparison a certain amount of discrepancy is expected, since the presented model is focused on the dynamics of the driveline and does not account for the dynamics of the two frames. This aspect is enlightened also by the fact that the accuracy of the estimation tends to decrease by increasing the nominal speed, which also cause the influence of the dynamics of the frames to increase. On the basis of this considerations, the comparison demonstrates that the dynamic behavior of the machine is well captured by the proposed model, even if a full dynamic characterization of the frames has been avoided with the aim at not increasing the complexity of the approach unnecessarily.

5 Concluding remarks

In the present work, a dynamic model of a linear vibrating feeder has been developed and validated by experimental measurements. Departing from the geometrical analysis of the mechanism, the equations of motion for the estimation of the torsional dynamics of the system have been deduced. Moreover, a simplified version of the model has been proposed, in order to obtain an analytical formulation of the kinematic laws of the frames. The proposed mathematical formulation is generic and it is valid for arbitrary design data, as different inertia terms, geometrical dimensions and number of frames.

Furthermore, a dedicated experimental campaign has been conducted on a real linear feeder, with the aim at characterizing the dynamic behavior of the driveline and the frames in operational conditions.

Eventually, the model has been successfully validated under different working conditions in terms of both translational and torsional vibrations, by taking advantage of the data obtained from the experimental

campaign. Comparison of the time domain data and RMS values of both the instantaneous speed and the translational vibration has shown the quality of the estimation provided by the presented model.

On the basis of this analysis, the model can be considered as a useful tool to predict the influence of various design parameters on the NVH behavior of the machine, i.e. reduction of the crankshaft speed variation causing undesired high vibration level, estimation of the global vibration level of the frames and determination of the applied variable torque on the designed driveline.

References

[1] M.A. Parameswarant, Vibratory Conveying--Analysis and Design: A Review, 14 (1979) 89–97.

[2] E. Mucchi, R. Di Gregorio, G. Dalpiaz, Elastodynamic analysis of vibratory bowl feeders: Modeling and experimental validation, Mech. Mach. Theory. 60 (2013) 60–72. doi:10.1016/j.mechmachtheory.2012.09.009.

[3] X. Ding, J.S. Dai, Characteristic equation-based dynamics analysis of vibratory bowl feeders with three spatial compliant legs, IEEE Trans. Autom. Sci. Eng. 5 (2008) 164–175. doi:10.1109/TASE.2007.910301.

[4] Ž. V. Despotović, D. Urukalo, M.R. Lečić, A. Ćosić, Mathematical modelling of resonant linear vibratory conveyor with electromagnetic excitation: simulations and experimental results, Appl. Math. Model. 0 (2016) 1–24. doi:10.1016/j.apm.2016.09.010.

[5] R. Silversides, J.S. Dai, L. Seneviratne, Force Analysis of a Vibratory Bowl Feeder for Automatic Assembly, J. Mech. Des. 127 (2005) 637. doi:10.1115/1.1897407.

[6] G.H. Lim, Vibratory feeder motion study using Turbo C++ language, Adv. Eng. Softw. 18 (1993) 53–59. doi:10.1016/0965-9978(93)90007-G.

[7] G.P. Maul, M. Brian Thomas, A systems model and simulation of the vibratory bowl feeder, J. Manuf. Syst. 16 (1997) 309–314. doi:10.1016/S0278-6125(97)88461-0.

[8] G.H. Lim, On the conveying velocity of a vibratory feeder, Comput. Struct. 62 (1997) 197–203. doi:10.1016/S0045-7949(96)00223-4.

[9] J.A. Vilán Vilán, A. Segade Robleda, P.J. García Nieto, C. Casqueiro Placer, Approximation to the dynamics of transported parts in a vibratory bowl feeder, Mech. Mach. Theory. 44 (2009) 2217–2235. doi:10.1016/j.mechmachtheory.2009.07.004.

[10] M. Ramalingam, G.L. Samuel, Investigation on the conveying velocity of a linear vibratory feeder while handling bulk-sized small parts, Int. J. Adv. Manuf. Technol. 44 (2009) 372–382. doi:10.1007/s00170-008-1838-1.

[11] S. Ganapathy, M.A. Parameswaran, Effect of material loading on the starting and transition over resonance of a vibratory conveyor, Mech. Mach. Theory. 22 (1987) 169–176. doi:http://dx.doi.org/10.1016/0094-114X(87)90041-3.

[12] H. Ashrafizadeh, S. Ziaei-Rad, A numerical 2D simulation of part motion in vibratory bowl feeders by discrete element method, J. Sound Vib. 332 (2013) 3303–3314. doi:10.1016/j.jsv.2013.01.020.

[13] A.I. Ribić, Ž. V. Despotović, High-performance feedback control of electromagnetic vibratory feeder, IEEE Trans. Ind. Electron. 57 (2010) 3087–3094. doi:10.1109/TIE.2009.2037677.

[14] X. Kong, X. Zhang, X. Chen, B. Wen, B. Wang, Phase and speed synchronization control of four eccentric rotors driven by induction motors in a linear vibratory feeder with unknown time-varying load torques using adaptive sliding mode control algorithm, J. Sound Vib. 370 (2015) 23–42. doi:10.1016/j.jsv.2016.02.013.

[15] S.B. Choi, D.H. Lee, Modal analysis and control of a bowl parts feeder activated by piezoceramic actuators, J. Sound Vib. 275 (2004) 452–458. doi:10.1016/j.jsv.2003.10.008.

[16] M. Buzzoni, E. Mucchi, G. Dalpiaz, Improvement of the vibro-acoustic behaviour of vibratory feeders for pasta by modelling and experimental techniques, in: Internoise 2016, Hamburg, 2016: pp. 4005–4013.

[17] R. Eksergian, Dynamical Analysis of Machines, Clark University,Worcester, MA, 1928.

315 [18] R. Di Gregorio, A Novel Dynamic Model for Single Degree-of-Freedom Planar Mechanisms Based on Instant Centers, J. Mech. Robot. 8 (2015) 11013. doi:10.1115/1.4030986.

TABLES

320

Table 1. List of the main parameters used for the simulation.

Leaf spring length c	0.448 m
Rod length b	1.446 m
Crank length e	0.0075 m
Leaf spring Young's module E	18 GPa
Driving side pulley radius R_1	0.047 m
Crankshaft side pulley radius R_2	0.131 m
Global inertia on the driving side J_2	0.164 kg*m^2
Mass of frame I m^I	1032.4 kg
Mass of frame II m^{II}	953.2 kg
Electric motor characteristic k_m	9.06 Nm*s/rad
Belt stiffness k	65000 N/m

FIGURES

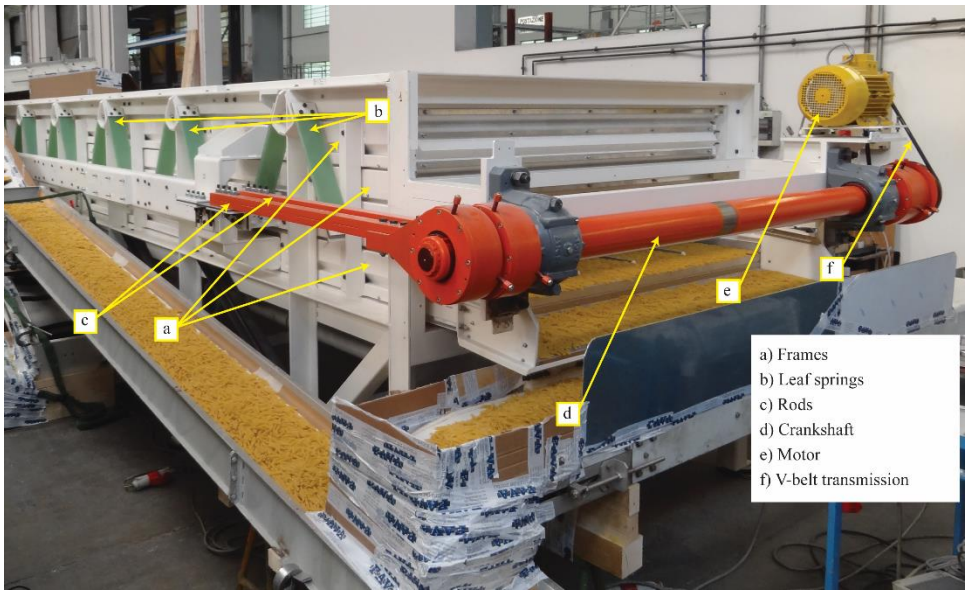

Figure 1. Photo of a real linear feeder highlighting its main components.

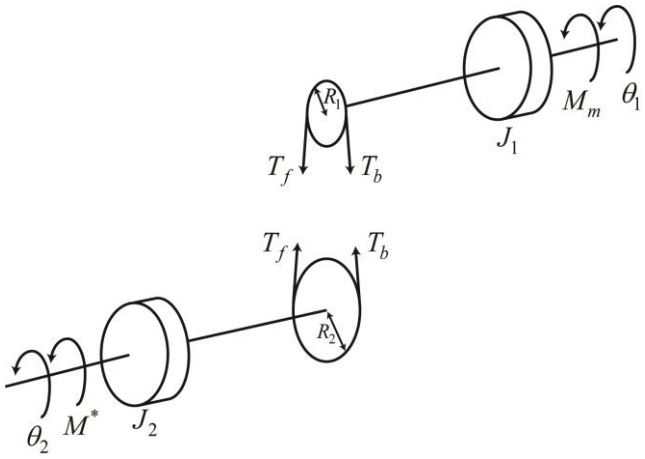

330

Figure 2. Dynamic model of the linear feeder divided in two subsystems.

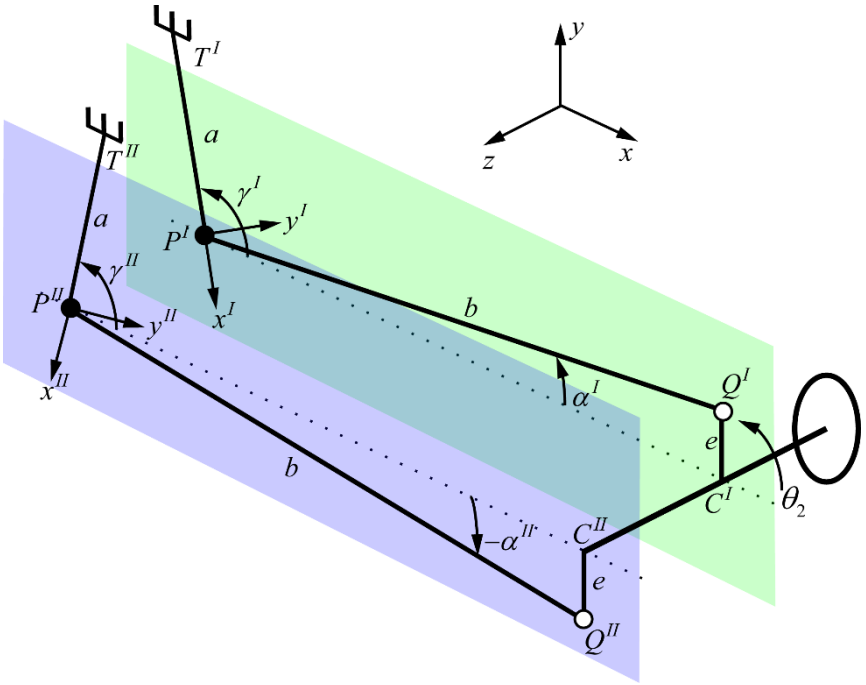

Figure 3: Schematic of the feeder transmission.

335

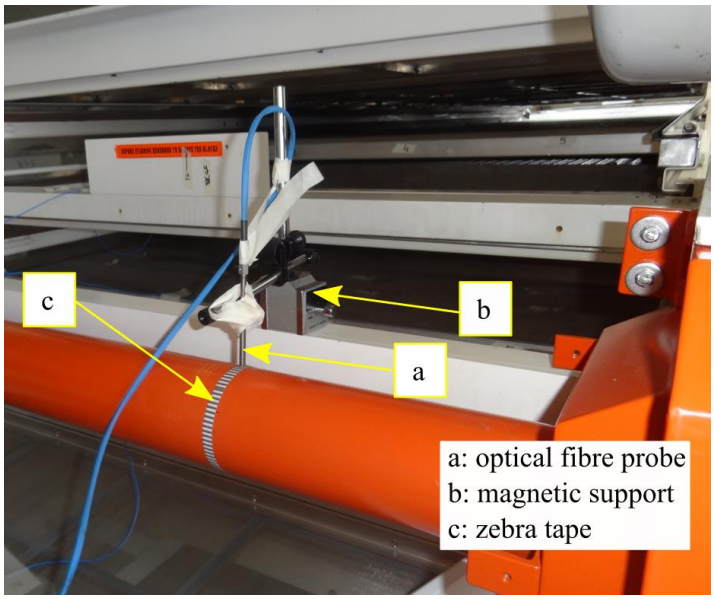

Figure 4: Setup for the torsional vibration measurement.

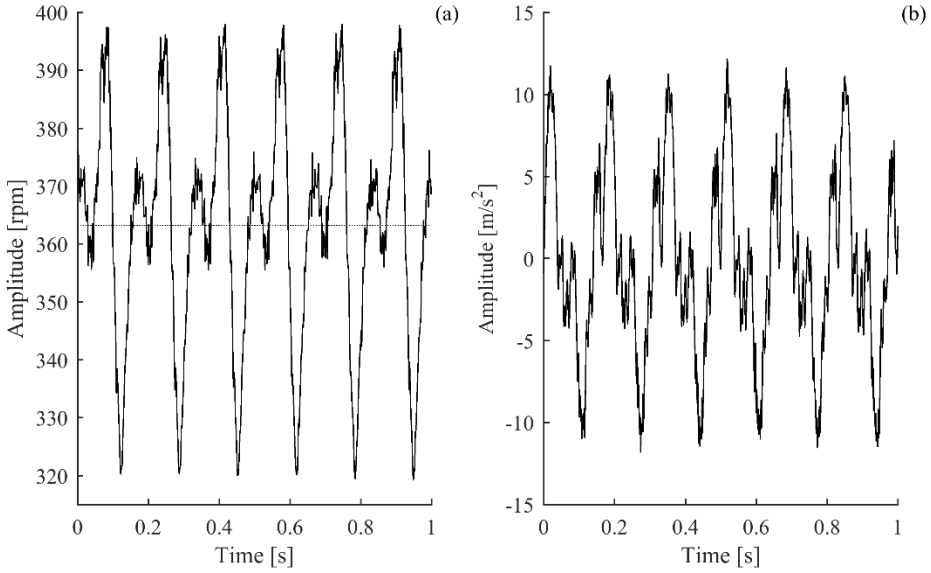

340 *Figure 5: examples of (a) the instantaneous speed and (b) the vibration signal of the frame I, at the nominal speed of 360rpm.*

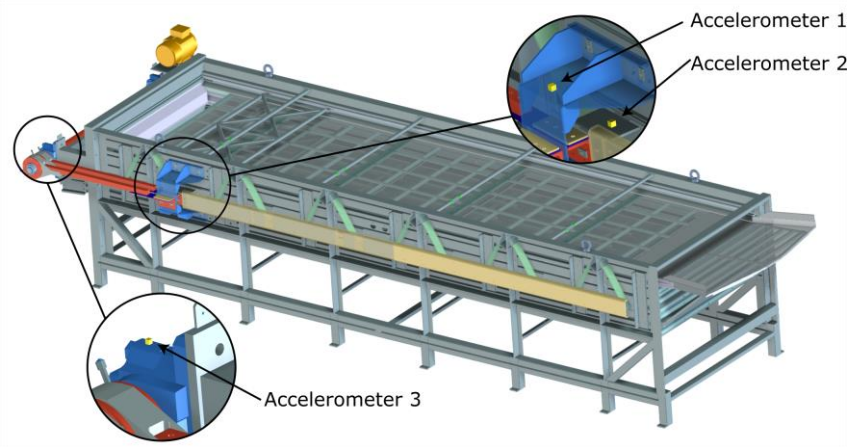

Figure 6: Accelerometers setup.

345

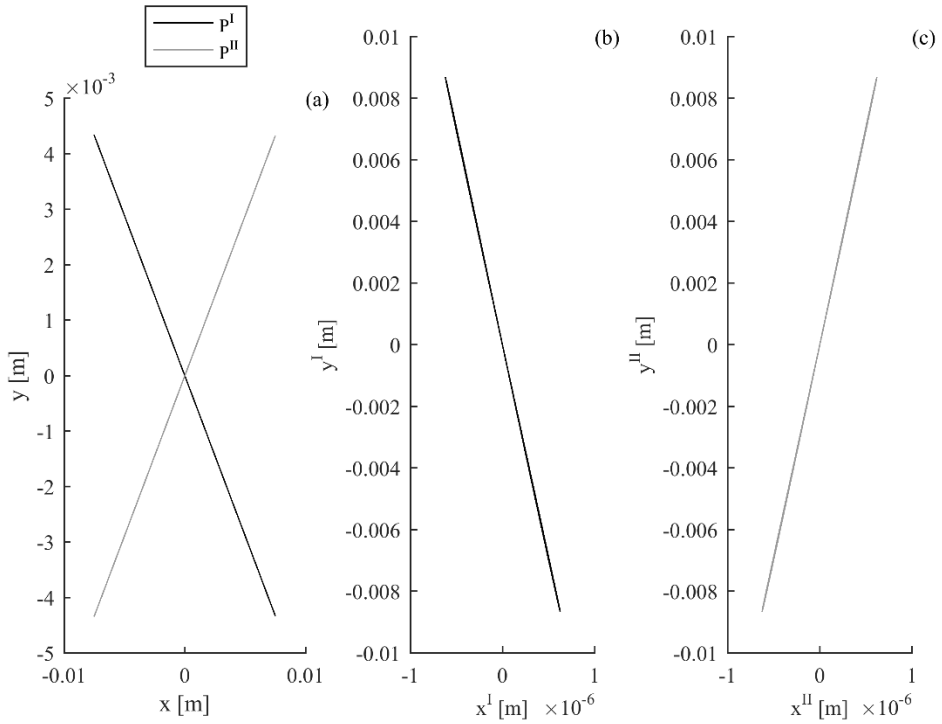

Figure 7: Trajectories described by P^I and P^{II} in a complete revolution of the crankshaft in (a) the global reference frame, (b) in the local reference frame of P^I and (c) in the local reference frame of P^{II} .

350

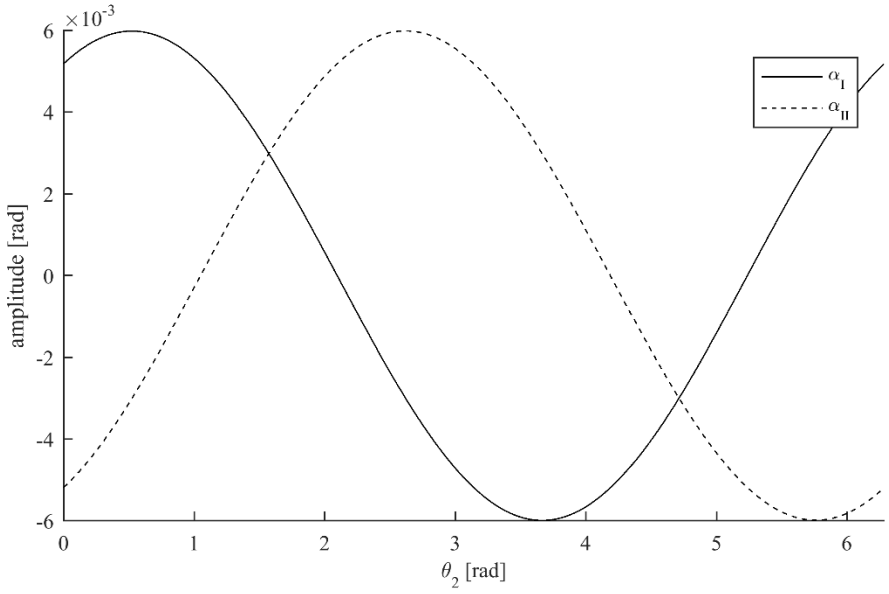

Figure 8: Values of α related to frame I and frame II in a complete revolution of the eccentric shaft with the Original model.

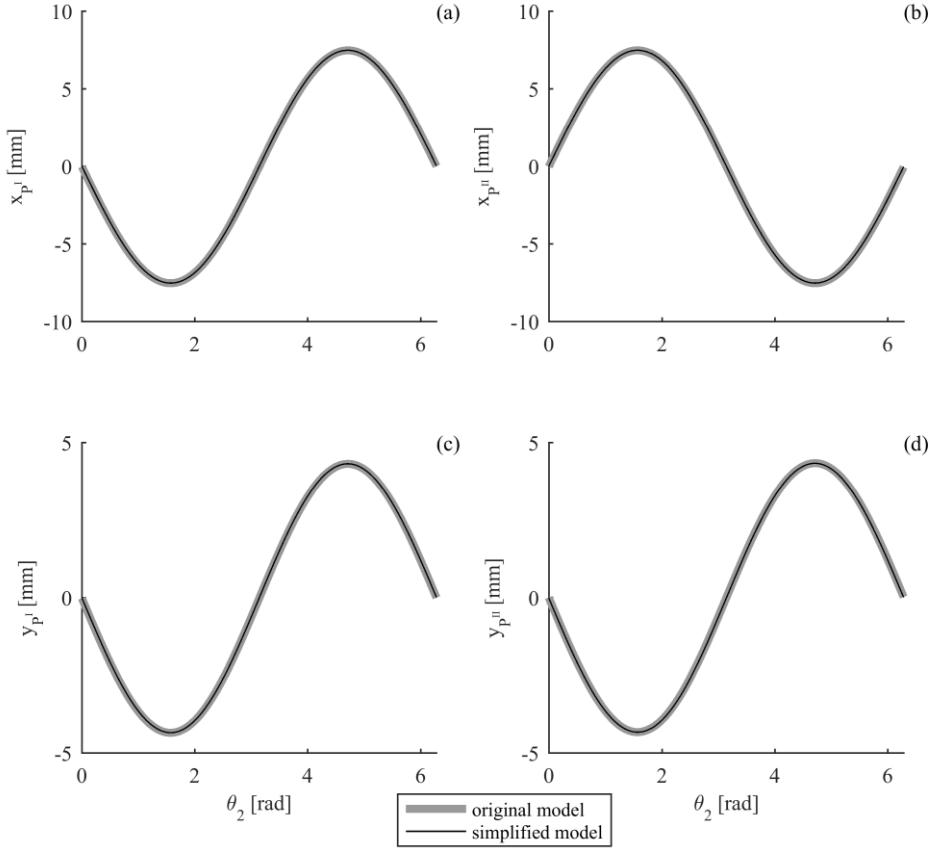

Figure 9: Kinematic displacements of (a) frame I in x direction, (b) frame I in x direction, (c) frame II in y direction and (d) frame II in y direction.

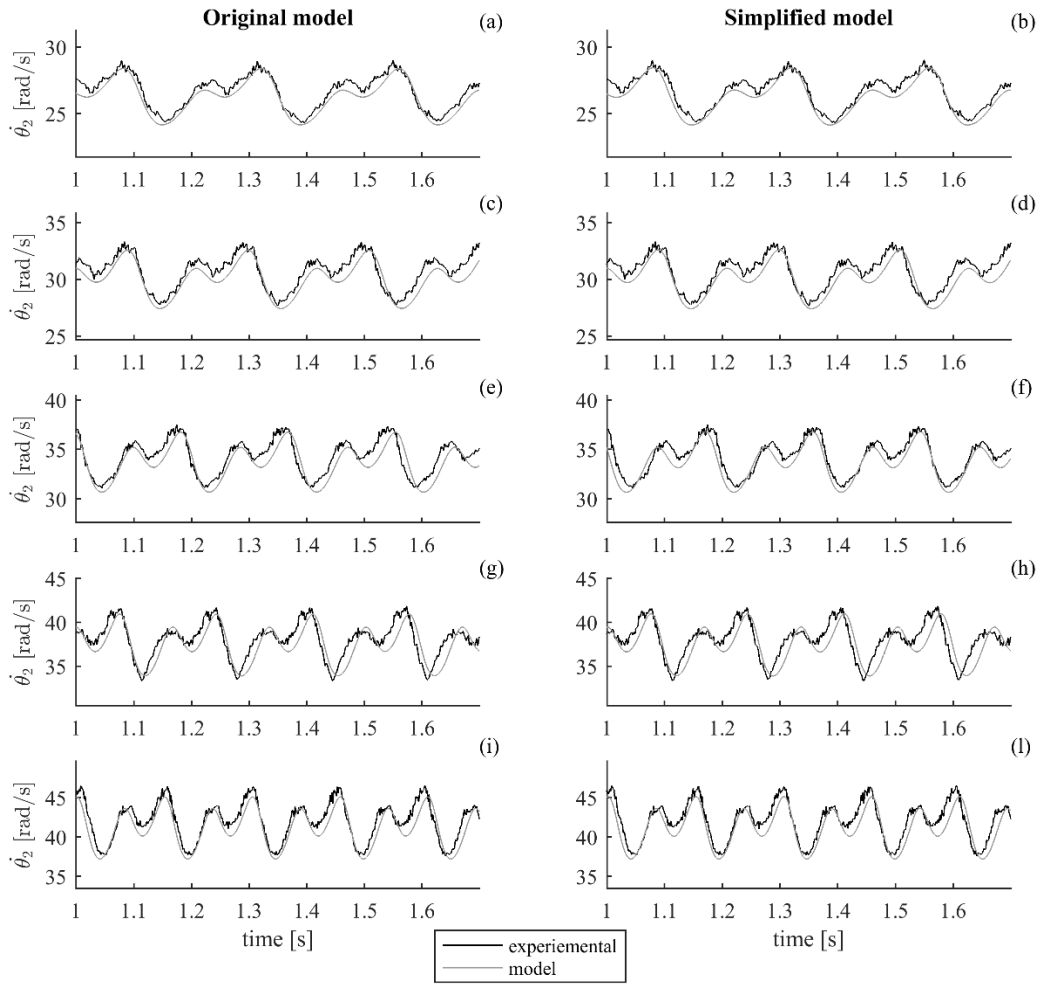

Figure 10. Instantaneous angular speed of crankshaft calculated with the Original model and the Simplified model in comparison with the measured data at the following power line frequencies: (a-b) 35 Hz, (c-d) 40 Hz, (e-f) 45 Hz, (g-h) 50 Hz, (i-l) 55 Hz.

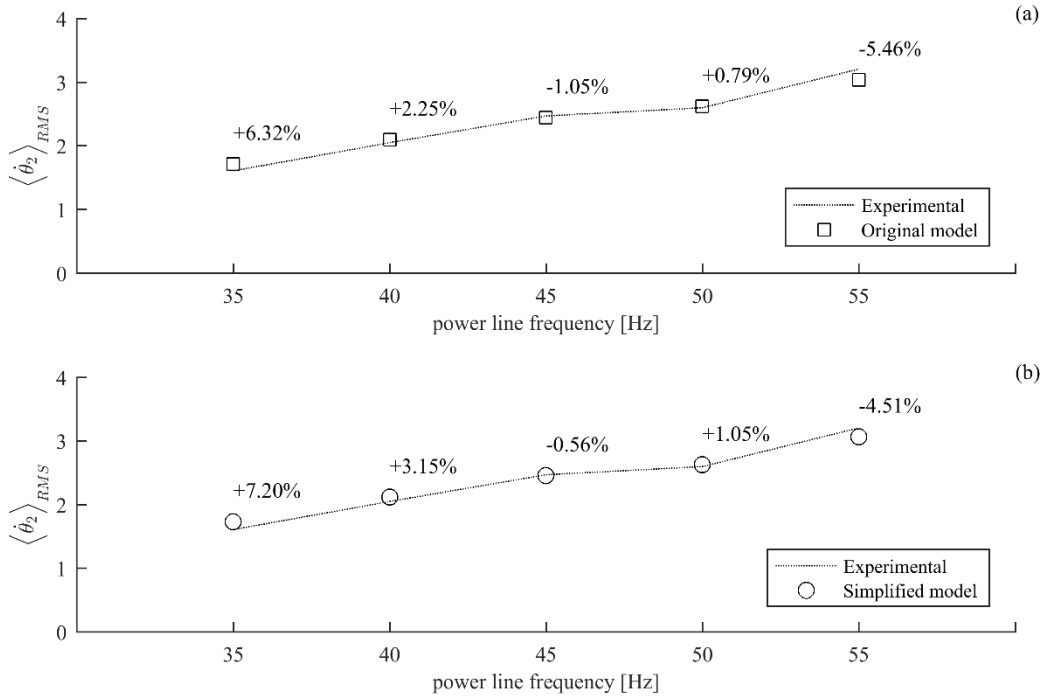

Figure 11. Comparison between experimental data and simulated results, calculated by means of (a) Original model and (b) Simplified model, in terms of the RMS value calculated on the first 4 harmonics of the crankshaft rotational speed.

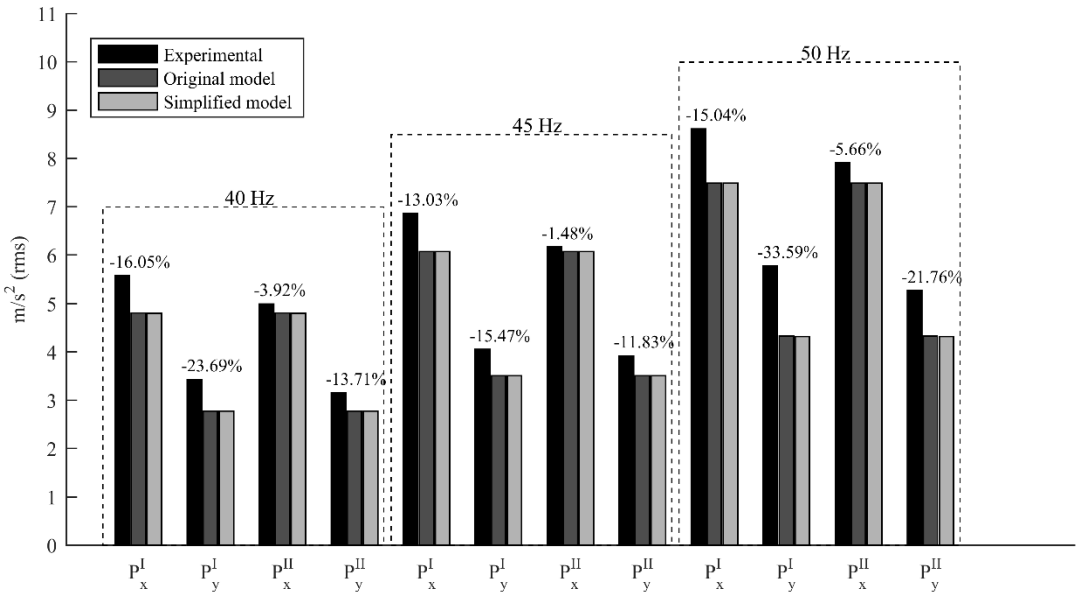

Figure 12. Comparison between experimental data and simulated results, in terms of RMS value of the vibration of the two frames for three different power line frequencies, i.e. three different nominal speed values of the crankshaft. The percentage values on the top of the bars refer to the maximum percentage differences between the model results and the experimental ones.